Astron. Astrophys. 319, 459–469 (1997)

ASTRONOMY
AND
ASTROPHYSICS

X-ray observations of the Magellanic-type Galaxy NGC 4449

A. Vogler and W. Pietsch

Max-Planck-Institut für extraterrestrische Physik, Gießenbachstraße, D-85748 Garching, Germany

Received 24 April 1996 / Accepted 30 July 1996

Abstract. X-ray emission ($L_x \sim 2.5 \times 10^{39}$ erg s^{-1}) from the nearby, face-on Magellanic-type irregular galaxy NGC 4449 was detected with the ROSAT PSPC and HRI. The HRI resolves seven point sources located within the D_{25} ellipse of the galaxy. The most luminous source is a supernova remnant detected with an intrinsic luminosity of $L_x = 4.7 \times 10^{38}$ erg s^{-1}. Another very luminous source ($L_x = 3.1 \times 10^{38}$ erg s^{-1}) is located between two Hα shells. A source near the southern border of the galaxy ($L_x = 1.7 \times 10^{38}$ erg s^{-1}) shows flux variations between the HRI and PSPC observations of a factor of two, no counterparts in other wavelengths and most likely is an X-ray binary. Two fainter sources ($L_x = 1.2 \times 10^{38}$ erg s^{-1} and $L_x = 0.8 \times 10^{38}$ erg s^{-1}) are positioned at the border of regions that show enhanced blue emission. The center of the galaxy was detected with a luminosity of $L_x = 7 \times 10^{37}$ erg s^{-1}.

Combining the spatial resolution of the HRI and the spectral capabilities of the PSPC indicates that the total X-ray emission of NGC 4449 is composed of resolved point sources ($L_x = 1.4 \times 10^{39}$ erg s^{-1}), unresolved point sources ($L_x = 2 \times 10^{38}$ erg s^{-1}), and extended emission possibly arising from a hot ($T \sim 3 \times 10^6$ K) gaseous component of the interstellar medium ($L_x = 1.0 \times 10^{39}$ erg s^{-1}). The spectral and spatial findings indicate that most of the thermal emission originates from parts in the outer HI disk and above it. The parameters and implications of a possible gaseous halo component are discussed.

The NGC 4449 X-ray emission components are compared with those of the Magellanic Clouds which can be resolved in the contributing X-ray emission components. The NGC 4449 point source and extended emission components seem to reflect the LMC scaled for the different galaxy masses.

Key words: galaxies: individual: NGC 4449 – galaxies: irregular – X-rays: galaxies

1. Introduction

The Magellanic-type irregular galaxy NGC 4449 is known for star formation activity associated with OB associations, giant HII regions, large-scale Hα filamentary structures, supernovae (and remnants), as well as a high gas content in the disk (cf., e.g. Hunter 1984, Hunter & Gallagher 1990 and 1992, Bothun 1986, Sabbadin et al. 1984). Hill et al. (1994) concluded from Hα and far-ultraviolet observations that a period of continuous star formation ended 5–6 Myr ago. The bar was the predominant site of star formation. During the same period, sporadic single-burst star formation events occured in the outer arms. Starting $\sim$ 5 Myr ago, star formation occurs around the northern periphery of the galaxy. Previously known parameters of NGC 4449 are listed in Table 1.

In X-rays NGC 4449 was detected with the IPC and HRI detector on-board of the *Einstein* satellite at a luminosity of 2.1 and 3.3×10^{39} erg s^{-1}, respectively (Fabbiano et al. 1992), corrected for our assumed distance of 3.7 Mpc. While the IPC could not resolve the galaxy, the deep HRI image taken in December 1979 reveals 3 point sources (HEASARC HRIEXO catalog). One of them coincides with a very luminous supernova remnant in NGC 4449 which was detected in the radio regime by Seaquist & Bignell (1978) and radiates in X-rays at a luminosity of 5×10^{38} erg s^{-1}(Blair et al. 1983).

We observed NGC 4449 in X-rays with the ROSAT HRI. The HRI detector provides high spatial resolution of the X-ray emission (point spread function $\sim 5''$) and allows to separate point sources within NGC 4449. To add spectral studies we retrieved PSPC data from the ROSAT public archive. Both observations were centered on NGC 4449.

2. Observations

NGC 4449 was observed with the HRI for 15.4 ks in four observation intervals (OBIs) on December 8 and 9, 1994. For a description of the satellite and the detectors aboard cf. Trümper (1983). The PSPC observations (7.8 ks) were carried out in 5 OBIs from November 21 to 23, 1991. Assuming a 5 keV thermal bremsstrahlung spectrum, both, the HRI and PSPC observations, reach a detection limit for point sources in NGC 4449 of $L_x \sim 5 \times 10^{37}$ erg s^{-1}. Attitude solutions of ROSAT pointings suggested by the Standard Analysis Software System (SASS, Voges 1992) show residual errors in the order of $6''$ (boresight error). To improve the attitude solution of the ROSAT HRI observation we used bright point sources visible in each OBI to align the different OBIs with respect to the first OBI, no offset was exceeding $4''$. The resulting attitude solution was tested

Send offprint requests to: W. Pietsch, (wnp@mpe-garching.mpg.de)

Table 1. Parameters of NGC 4449

		Ref.
Type	I(B)m	*
Assumed distance	3.7 Mpc (hence $1' \widehat{=} 1.1$ kpc)	♯
Position of center (2000.0)	R.A. $12^h28^m11^s.1$ Dec. $44°05'40''$	♯
D_{25}	$5'.4$	*
Corrected D_{25}	$5'.1$	*
Axial ratio	0.77	*
Position angle	45°	‡
Inclination	43°	*
Galactic foreground N_H	1.2×10^{20} cm^{-2}	§

References:
* Tully (1988)
♯ Bajaja et al. (1994)
‡ SIMBAD data base, operated at CDS, Strasbourg, France
§ Dickey & Lockman (1990)

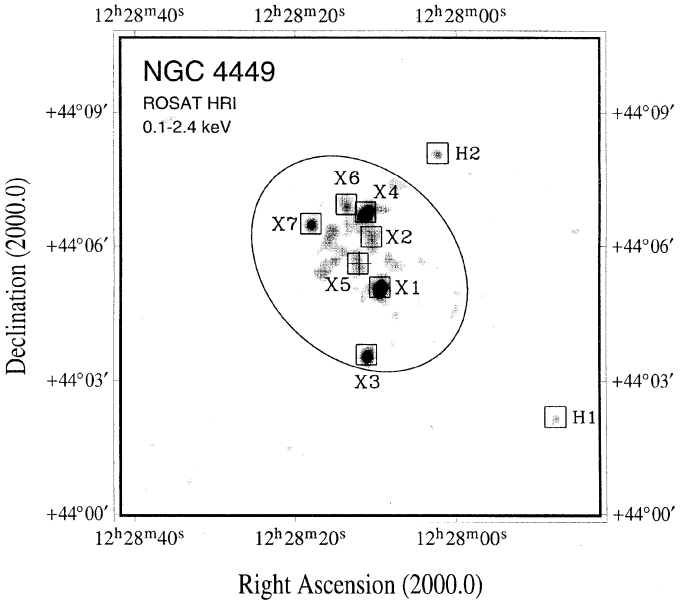

Fig. 1. Grey scale image of the X-ray flux seen with the ROSAT HRI for the central $10'.6 \times 10'.6$ of the NGC 4449 field. The image was constructed with a pixel size of $2''.5$ and smoothed with a Gaussian of $12''$ (FWHM). The center of NGC 4449 is marked with a cross, the D_{25} ellipse is indicated, and point sources (likelihood $L \geqq 8$) are enclosed by boxes and numbered

comparing X-ray point sources and possible optical counterparts suggested by the APM charts (Irwin 1994). After translating the X-ray coordinates $4''$ to the north (no rotation correction was performed) a close accordance of X-ray and optical sources could be established (remaining systematic error of the attitude solution about $4''$). The (corrected) center of the HRI field was at $\alpha = 12^h28^m12^s.0$ and $\delta = 44°05'28''$ (2000.).

A similar procedure for the PSPC data suggested a pointing correction $7''$ to the north and $2''$ to the west. The (corrected) center of the PSPC field was at $\alpha = 12^h28^m11^s.9$ and $\delta = 44°05'17''$ (2000.) with an remaining error of $4''$.

3. Data reduction

Data reduction was performed with the EXSAS software package (Zimmermann et al. 1992). For both, the HRI and PSPC data, we described our analysis procedures in Vogler & Pietsch (1996).

3.1. HRI observation

Fourteen point sources with a likelihood $L \geqq 8$ were detected in the HRI field of view. Maximum likelihood values (L) can be converted into probabilities (P) through $P = 1 - e^{-L}$, $L = 8$ corresponds to a Gaussian significance of 3.6σ (Cruddace et al. 1988; Zimmermann et al. 1994). Fig. 1 shows the inner $10'.6 \times 10'.6$ field of the HRI image. The center of the galaxy is indicated by a cross, and the D_{25} ellipse demonstrates the optical extent of the galaxy. Detected X-ray sources are marked with squares. Seven sources are found within the D_{25} diameter of NGC 4449 (X1, ..., X7). Their X-ray properties are summarized in Table 2: source number (col. 1), right ascension and declination (col. 2, 3), 90% confidence error radius of the source position (col. 4, including $4''$ systematic error for the attitude solution), likelihood of existence (col. 5), net counts and error for the 0.1–2.4 keV ROSAT band (col. 6), count rates and error after applying deadtime and vignetting corrections (col. 7). Three sources (X1, X2, and X4) were flagged as extended, their FWHM slightly exceeds the HRI point spread function (PSF) and the extension is given in column 8 (likelihood $L_{ext} \geq 10$). However, due to the low photon statistics of the HRI observation it is difficult to decide, if this extent is real or due to remaining errors in the attitude solution of the individual OBIs.

3.2. PSPC observation

Point sources were searched for using the five standard energy bands "broad" (0.11–2.40 keV), "soft" (0.11–0.41 keV), "hard" (0.52–2.01 keV), "hard1" (0.52-0.90 keV), and "hard2" (0.91-2.01 keV). For the inner field of the detector the hard band PSF has a full FWHM of $\sim 24''$, the soft band PSF has a FWHM of $\sim 45''$. We accepted sources with a likelihood of existence $L \geqq 8$. Fig. 2 shows the PSPC broad band contours for a $10'.6 \times 10'.6$ field centered on NGC 4449 (similar to Fig. 1). Several point sources are embedded in extended diffuse emission features, complicating a search for point sources within NGC 4449. Therefore we used the (marked) HRI positions as

Table 2. X-ray properties of HRI detected sources within the D_{25} ellipse of NGC 4449

Source	ROSAT name	R.A. (2000.0)	Dec. (2000.0)	R_{err}	Lik.	Net counts	Count rate	extent Lik., FWHM
	(RX J)	(h m s)	(° ′ ″)	(″)			(10^{-4} cts s^{-1})	
(1)	(2)	(3)	(4)	(5)	(6)	(7)	(8)	(9)
X1	122809.4+440509	12 28 09.48	+44 05 09.5	4.3	150.7	76.7 ± 9.2	50.5 ± 6.0	19.0, 7.5″
X2	122810.5+440616	12 28 10.54	+44 06 16.5	6.7	8.6	24.3 ± 6.0	16.0 ± 4.0	10.0, 14.0″
X3	122811.1+440339	12 28 11.15	+44 03 39.0	4.3	87.5	41.5 ± 6.7	27.3 ± 4.4	
X4	122811.2+440649	12 28 11.29	+44 06 49.5	4.6	79.6	72.9 ± 9.2	48.1 ± 6.1	38.9, 11.8″
X5	122812.2+440541	12 28 12.20	+44 05 41.0	6.9	9.3	17.8 ± 5.1	11.7 ± 3.4	
X6	122813.6+440700	12 28 13.64	+44 07 00.0	6.4	15.7	18.7 ± 5.1	12.4 ± 3.4	
X7	122818.0+440634	12 28 18.05	+44 06 34.0	4.4	47.7	24.8 ± 5.3	16.3 ± 3.5	

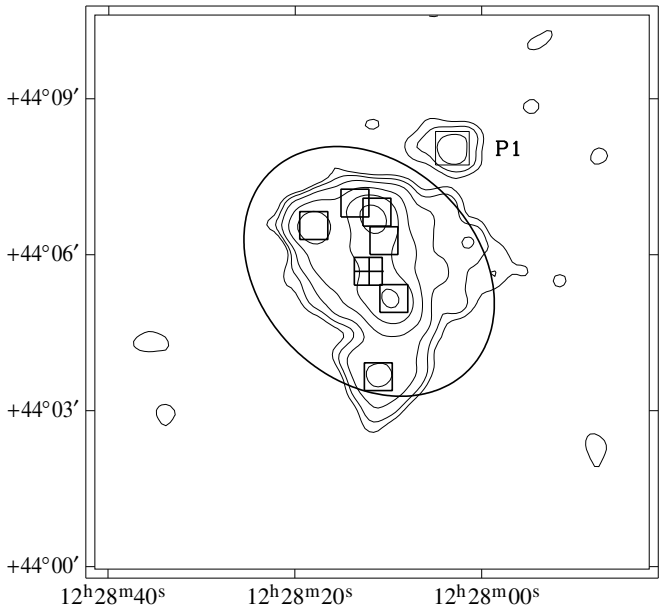

Fig. 2. Contour plot of the broad band ROSAT PSPC image of NGC 4449. Contours are 2, 3, 5, 9, 15, and 31σ above the background ($1\sigma \;\widehat{=}\; 7.9 \times 10^{-4}$ cts s^{-1} arcmin^{-2}, background $\widehat{=}\, 1.51 \times 10^{-3}$ cts s^{-1} arcmin^{-2}). For orientation the positions of the HRI detected sources are marked, the optical center of NGC 4449 is marked as a cross. The ellipse demonstrates the optical extent of the galaxy (D_{25} ellipse)

input for a source search within the D_{25} ellipse of the galaxy (cf. Sect. 4.1).

4. Results

4.1. Comparing the HRI and PSPC measurement

Extended X-ray emission visible in the PSPC image (cf. Fig. 2) complicates the point source detection in NGC 4449. This may be due to some bright point sources detected by the HRI with separations smaller than the PSPC PSF, additional point sources below the detection limit and diffuse emission as expected from a hot gaseous component of the interstellar medium. We took the source positions of the HRI detections as an input list for PSPC source detection. Table 3 gives the results: the separation of the source position as suggested by the 'multi source fit technique' (cf. Zimmermann et al. 1994) and the HRI measured source position (col. 2), the likelihood of the source (col. 3), the net counts in the broad band (col. 4), the hardness ratios (col. 5 and col. 6, using the net counts in the different PSPC bands: HR1 = (hard–soft)/(hard+soft) and HR2 = (hard2–hard1)/(hard2+hard1)), and the count rate (col. 7). The bright sources X1, X3, and X4 coincide within the position errors with the 3 *Einstein* HRI point sources listed in the HEASARC HRIEXO catalog.

In Table 4 we compare the fluxes and luminosities for all point sources as measured with the HRI and PSPC detector in December 1994 and November 1991, respectively. We give for both detectors the flux and luminosity of the sources. A 5 keV thermal bremsstrahlung spectrum was assumed to convert the count rates to fluxes. The conversion factors for the 0.1–2.4 keV band are 3.76×10^{-11} erg cm^{-2} cts^{-1} and 1.28×10^{-11} erg cm^{-2} cts^{-1} for the HRI and PSPC, respectively (corrected for Galactic absorption, 0.1–2.4 keV band). These conversion factors may change by $\sim 15\%$ if other spectral models are used (as estimated, e.g. in Vogler et al. 1996b). To convert *Einstein* HRI count rates (0.5–4 keV) into fluxes in the ROSAT band (0.1–2.4 keV) for a spectrum as given above we used an conversion factor of 6.9×10^{-11} erg cm^{-2} cts^{-1}.

For most sources ROSAT PSPC and HRI derived luminosities match within the errors, only for X3 and X7 the difference exceeds the 1σ error of the measurements. This may either be explained by time variability over the 3 years time span of the PSPC and HRI observations or due to an assumed wrong spectral model. NGC 4449 was observed with the HRI detector aboard the *Einstein* satellite 12 years before the ROSAT PSPC observations. For X1 the HEASARC HRIEXO count rate is $(2.2 \pm 0.4) \times 10^{-3}$cts s^{-1} corresponding to a flux in the ROSAT band that is comparable within the errors with the ROSAT derived values, X3 was bright during the *Einstein* observation ($(1.1 \pm 0.3) \times 10^{-3}$cts s^{-1}, flux similar as detected with the ROSAT HRI). The flux of X4 derived from the *Ein-*

Table 3. X-ray properties of PSPC detected sources inside the D_{25} ellipse of NGC 4449

	Δ_{P-H} ($''$)	Lik.	Net counts	HR1	HR2	count rate (10^{-3} cts s^{-1})
(1)	(2)	(3)	(4)	(5)	(6)	(7)
X1	4	209.8	112.6 ± 16.5	+0.2±0.2	−0.1±0.2	14.0 ± 2.0
X2	2	56.4	45.3 ± 11.9	+0.3±0.3	−0.3±0.3	5.5 ± 1.4
X3	5	30.3	27.1 ± 9.1	−0.6±0.4	−1.0±0.0	3.3 ± 1.1
X4	9	228.8	123.9 ± 17.2	+0.7±0.2	+0.5±0.2	15.5 ± 2.1
X5	15	54.3	42.3 ± 11.0	+0.1±0.3	−0.2±0.3	5.1 ± 1.3
X6	9	30.2	29.8 ± 10.0	+0.3±0.3	+0.2±0.3	4.0 ± 1.4
X7	4	111.0	65.0 ± 12.6	+0.5±0.2	+0.6±0.3	9.0 ± 1.8

stein measurements is comparable to the ROSAT flux (Blair et al. 1983, see Sect. 5.1).

The brightest sources in NGC 4449, X1 and X4, have X-ray luminosities of $L_x \sim 3 \times 10^{38}$ erg s^{-1}. The hardness ratios of X1 indicate moderate absorption (HR1=+0.2) and rather soft spectral behavior (HR2=–0.1). On the other hand, source X4 seems to be highly absorbed (HR1=+0.7) and to possess a harder spectrum (HR2=+0.5). Two fainter sources, X2 and X6, are detected close to X4. Both sources show luminosities around 1×10^{38} erg s^{-1}. HR1=+0.3 for X2 and for X6 suggests lower absorption than measured for X4, HR2=–0.3 and +0.2, respectively, indicate softer spectra than suggested for X4. Nevertheless, the low count rates for X2 and X6 introduce greater errors to the calculated hardness ratios and thus these ratios are only helpful for a first estimate. The X-ray source X5 coincides spatially with the optical center of the galaxy and is detected with a luminosity of $L_x = 0.7 \times 10^{38}$ erg s^{-1}.

To investigate the HRI observation for diffuse emission structures, we calculated an X-ray map with the help of an adaptive filtering technique (cf., e.g. Vogler & Pietsch 1996). The adaptive filtered HRI as well as the soft and hard1 PSPC maps show extended emission features in addition to the detected point sources (Fig. 3). The positions of the point sources are marked by squares in all figures according to Table 2, the D_{25} ellipse is indicated. A similar morphological appearance in the HRI and PSPC hard1 map is discernible for an area of extended emission centered $\sim 1'$ north of the galaxy's center with an extent of $\sim 4'$ diameter. The HRI map shows two arcs of extended emission protruding to the south west and to the south. The latter is traced also in the PSPC soft map; a curvature of the arc is visible in the HRI map, while the PSPC soft band shows a plateau like structure. The PSPC hard2 band mainly shows contributions of the point sources.

4.2. Time variability study of point sources

The spatial resolution of the HRI observation was used to separate point sources and to study the time variability of their emission. We performed a maximum likelihood search for the positions given in Table 2 during five observation blocks. Block 1, 2, and 5 are corresponding to OBI 1, 2, and 4; the integrated observation times are 1.7 ks, 2.6 ks, and 3.9 ks respectively. The third OBI (observation time 7.2 ks) was subdived in two blocks with 3.3 ks and 3.9 ks. Fig. 4 shows the count rates and errors, in the case of errors exceeding the count rate we give upper limits (2σ). Dashed lines indicate the averaged count rates calculated for the entire observation. Variations in count rates do not exceed the 2σ statistical error for any of the sources. Due to the low source count rates this however is no very stringent argument for a constant source intensity. Variability by factors of several (especially drops in source flux to zero during one observation block) would only result in an upper limit comparable to the average detected emission. Time variability on short scales by just a factor of two (as indicated on longer scale for X3 and X7 between the HRI and PSPC observations, see Sect. 4.1) would not have been significant.

4.3. Searching for counterparts of X-ray sources

We compared the X-ray source positions with maps in the optical (J, E, and O plate available from the Palomar and the Digitized Sky Survey, Hα maps from Hill et al. (1994) and references therein), radio (available from Condon (1987)), and far ultraviolet (FUV, Hill et al. 1994) regime. The radio map shows NGC 4449 as an extended radio source and does not allow a correlation of radio and X-ray point sources. Fig. 5 compares the ROSAT HRI map to Hα (a) and background subtracted blue emission (b). Both maps were reproduced from Hill et al. (1994). Image (a) shows several filamentary, loop-, knot- and shell-like structures. Some of these structures are numbered from '1' to '4' according to Hunter & Gallagher (1990, 1992), two long filaments are labeled 'a' and 'b' according to Hill et al. (1994), 'sh' marks a double Hα shell. Image (b) shows a patchy distribution of young associations and clusters. The background subtraction enhances the small scale features. 'B' indicates the position of a circular feature outlined in young stars. The feature apparently contains no bright stars inside of it and several authors (Bothun 1986, McCray & Kafatos 1987) point out that it may be a superbubble.

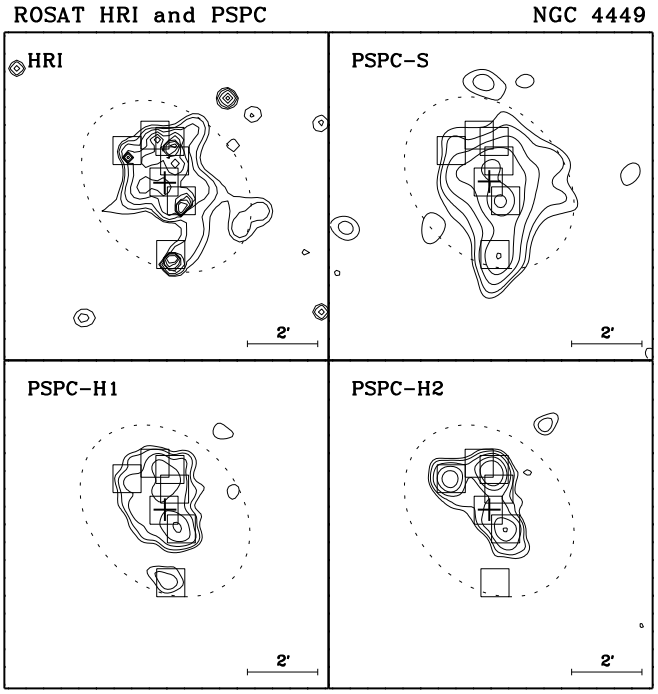

Fig. 3. *Upper left figure:* ROSAT HRI map obtained with help of an adaptive filtering technique (cf. Sect. 4.1). The contours are given in units of σ (5.4×10^{-4} cts s^{-1} arcmin^{-2}) above the background (5.3×10^{-3} cts s^{-1} arcmin^{-2}). The units are 2, 3, 5, 9, 15, 31, 63, and 127σ. *Other figures:* ROSAT PSPC maps in the bands soft (S), hard1 (H1), and hard2 (H2). The soft band contours are given in units of σ (4.3×10^{-4} cts s^{-1} arcmin^{-2}) above background (1.30×10^{-3} cts s^{-1} arcmin^{-2}); the units are 2, 3, 5, 8, 12, 15, and 20σ. Hard band contours are given (due to the negligible background in these bands) in units of 1.5 photons accumulated per 30″ diameter, one unit corresponds to 9.1×10^{-4} cts s^{-1} arcmin^{-2}; contours show 2, 3, 5, 9, and 15 units. The center of the galaxy is marked as cross, the optical D_{25} ellipse is indicated, source positions are marked according to Table 2

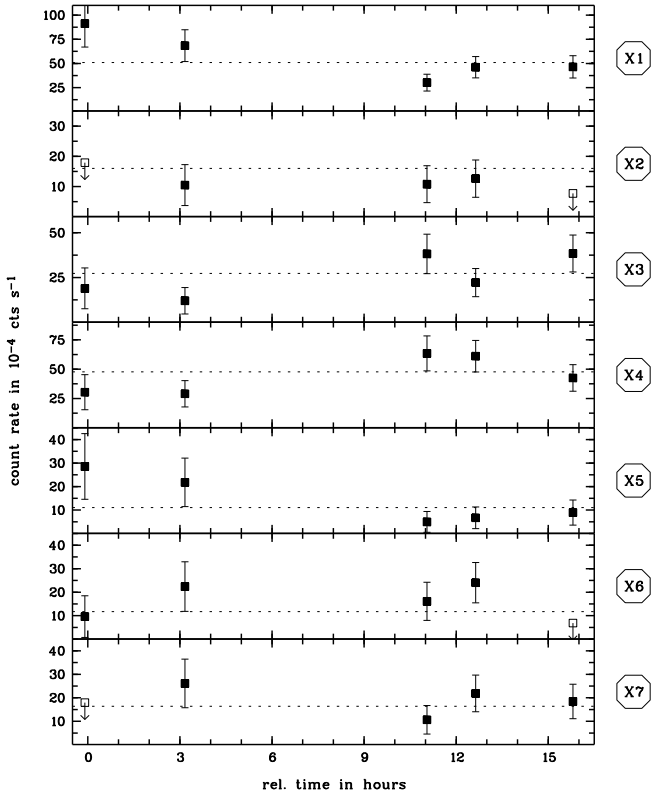

Fig. 4. Lightcurves for point sources in NGC 4449 as measured with the ROSAT HRI. The observation times are 1.7 ks, 2.6 ks, 3.3 ks, 3.9 ks, and 3.9 ks, respectively. Count rates are given as filled squares (1σ errors are indicated); if the 1σ error exceeds the count rate 2σ upper limits are given (open squares). Dashed lines give the averaged count rates calculated from the entire observation

4.3.1. Source X1: a source near the Hα double shell

Source X1 is located near the center of the Hα double shell (sh). The X-ray source position is offset by $\sim 8''$ ($\sim$ 140 pc) to the east from the center of the Hα double shell. Hill et al. (1994) zoom into this region in their Fig. 5. The shell boundaries have radii of 5.″4 ($\sim$ 97 pc) and 10.″8 ($\sim$ 190 pc). Our Fig. 5b shows a spatial coincidence between the X-ray source and young stellar associations or clusters. In addition, the source position coincides with the bright FUV source no. 18 of Hill et al. (1994). For an instantaneous burst model these authors estimate the cluster age and mass at 6.7×10^6 yr and 1.2×10^6 $M_\odot$, respectively. The observed X-ray luminosity of $L_x \sim 3 \times 10^{38}$ erg s^{-1} could be explained by the superposition of discrete X-ray sources contained in such a cluster. Already a few X-ray binaries, radiating at the Eddington limit of a solar mass neutron star, could explain the observed luminosity. On the other hand, the hardness ratios (HR1=+0.2 argues for medium absorption, and HR2=–0.1 for soft spectral behavior) may point to a thermal origin of the X-ray emission. Several mechanisms are possible. The radiation could be due to a young supernova remnant expanding into dense interstellar medium (ISM), associated e.g. with the shell of the stellar cluster (cf. also the discussion of X4 in Sect. 5.1). It could also be due to interactions of the Hα double shell and the stellar cluster, e.g. if a fragmentation in the 'walls' enables an outflow of hot gas from the interior of the shell.

4.3.2. Source X3

No counterpart for source X3 is visible in the Hα map (Fig. 5a), in the background subtracted blue plate (Fig. 5b) or other optical plates. Assuming a 5 keV thermal bremsstrahlung spectrum the difference of the detected flux in the HRI (f_x = $(10.3 \pm 1.7) \times 10^{-14}$ erg cm^{-2} s^{-1}) and PSPC measurement ($f_x = (4.3 \pm 1.4) \times 10^{-14}$ erg cm^{-2} s^{-1}) argues for a time variability of the X-ray flux and may be explained by the detection of an accretion powered object in the outer disk of NGC 4449 or by a background AGN. The maximum flux measured with the HRI corresponds to $L_x \sim (2.3 \pm 0.6) \times 10^{38}$ erg s^{-1} at the distance of NGC 4449. This luminosity slightly exceeds the Eddington limit for a one solar mass neutron star binary. On the other hand, the hardness ratios calculated from the PSPC measurement, HR1=–0.6 and HR2=–1.0, argue for low absorp-

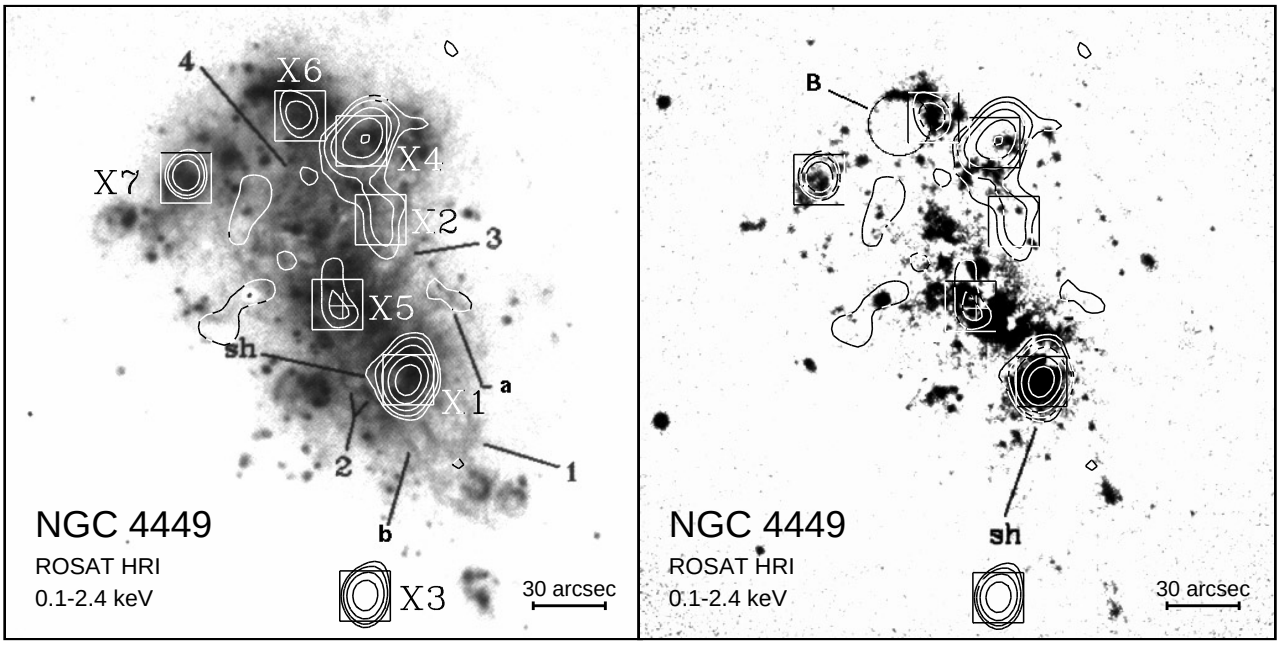

Fig. 5. ROSAT HRI X-ray contours overlaid onto an Hα (left side) and background subtracted blue image (right side). Both images are reproductions from Hill et al. (1994). The X-ray sources are marked by squares (source numbers are given in the left figure), the optical center of NGC 4449 is marked as cross. The Hα image shows several filamentary, loop-, knot- and shell-like structures. Some of these are numbered from *1–4* according to Hunter & Gallagher (1990, 1992), two long filaments are labeled with *a* and *b*- according to Hill et al. (1994), *sh* marks a double Hα shell. *B* indicates the position of a circular feature outlined in young stars. The ROSAT HRI contours were calculated from the image shown in Fig. 1, the levels are 2, 3, 5, 9, and 15σ above the background (background $\widehat{=}$ 2.5×10^{-3} cts s^{-1} arcmin^{-2}, $\sigma \widehat{=}$ 1.5×10^{-4} cts s^{-1} arcmin^{-2})

tion and soft spectral behavior of the source, as expected for a foreground object or a very soft source located in the outer disk or halo of NGC 4449. Then the assumed spectral model would be wrong and the time variability argument may vanish.

4.3.3. The central source X5

Source X5 (L_x = 7.2×10^{37} erg s^{-1}) coincides with the optical center of the galaxy. The luminosity may either be explained by the detection of a bright X-ray binary in the bulge of the galaxy or an accumulation of unresolved point sources or a low-luminosity active galactic nucleus. A detection of an active nucleus for the Magellanic-type irregular NGC 4449 would be unexpected, since other Magellanic-type galaxies do not possess a defined nucleus (cf. Sect. 5.3). However, for the LMC there are discussions, that the prominent star forming region 30 Dor may be identified with the center of the galaxy. The entire 30 Dor region is visible in PSPC pointings as a complex source with a total X-ray luminosity of $\sim 3 \times 10^{38}$ erg s^{-1} (Williams & Chu 1994). The source X5 might trace a similar accumulation of sources in NGC 4449. Strong variability of individual sources will only be reflected in small variability of the overall luminosity of the source complex. Indeed, the PSPC detected flux for source X5 was comparable to the HRI measurement.

4.3.4. The sources X2, X6, and X7

The sources X2, X6, and X7 have luminosities around 10^{38} erg s^{-1}. X6 and X7 have counterparts in the Hα and background subtracted blue map. Source X7 is centered on a circular pattern of knots in the background subtracted blue map, X6 is centered on an extended bright source in the blue map located on the western border of the superbubble (marked *B*) which was discovered by Bothun (1986).

The luminosities of all three X-ray sources are compatible with bright X-ray binaries. For this class of sources time variability of the X-ray flux can be expected. The limited photon statistics did not allow to draw clear conclusions on variability from the HRI measurement alone (cf. Fig. 4). PSPC and HRI fluxes exclude variations by more than a factor of three for all of the sources between the two observations (cf. Table 4); source X7 is a candidate for variability (cf. Sect. 4.1).

4.3.5. Source X4: detection of a supernova remnant

Source X4 coincides with a supernova remnant (SNR) first detected in radio observations (Seaquist & Bignell 1978) and optical observations (Balick & Heckman 1978), subsequent in X-ray (Blair et al. 1983) and ultraviolet (Blair et al. 1984).

For the HRI measurement X4 was flagged extended by the detection algorithm (cf. Table 2). The extent may be caused by the superposition of several point sources, misalignment of

Table 4. Comparison of HRI and PSPC results for point sources within the D_{25} ellipse of NGC 4449

	f_x *		L_x *	
	HRI	PSPC	HRI	PSPC
	(10^{-14} erg arcmin^{-2} s^{-1})		(10^{37} erg s^{-1})	
X1	19.0 ± 2.3	17.9 ± 2.6	31.0 ± 3.7	29.2 ± 4.3
X2	6.0 ± 1.5	7.0 ± 1.8	9.8 ± 2.4	11.4 ± 3.0
X3	10.3 ± 1.7	4.3 ± 1.4	16.7 ± 2.7	7.0 ± 2.3
X4	18.1 ± 2.3	19.8 ± 2.7	29.5 ± 3.7	32.3 ± 4.5
X5	4.4 ± 1.3	6.6 ± 1.7	7.2 ± 2.1	10.7 ± 2.8
X6	4.7 ± 1.3	5.2 ± 1.7	7.6 ± 2.1	8.4 ± 2.8
X7	6.1 ± 1.3	11.5 ± 2.2	10.0 ± 2.1	18.8 ± 3.7

* assuming a 5 keV thermal bremsstrahlung spectrum, corrected for Galactic absorption

the different OBIs, or a 'real' extent of a single point source. However, the photon statistics does not allow a final decision; the fluxes measured with the HRI and PSPC are in agreement. For further considerations we assume that the whole measured flux is due to the SNR. The absorbing column towards source X4 was estimated with help of a thermal bremsstrahlung fit to $N_H \sim 7 \times 10^{20}$ cm^{-2}, the suggested temperature was $T \sim 7 \times 10^6$ K. Due to the small separation of X2 and X6 from X4, photons of the possibly less high absorbed, softer sources X2 and X6 are contained in the spectrum of X4. Therefore, both values, N_H and T, should be viewed as lower limits.

4.3.6. Two X-ray sources near NGC 4449

RX J122802.3+440803 was detected about 3′ northwest of the galaxy's center with the HRI and PSPC. The source is labeled H2 in Fig. 1, it is labeled P1 in Fig. 2. The HRI position was α = 12^{h}28^{m}02^s.3 and δ = 44°08′03″, the PSPC detection was offset by 6″. The measured count rates (fluxes) for the HRI and PSPC detections were $(7.4 \pm 2.4) \times 10^{-4}$ cts s^{-1} (f_x = 2.8 × 10^{-14} erg cm^{-2} s^{-1}) and $(5.5 \pm 1.1) \times 10^{-3}$ cts s^{-1} (f_x = 7.2 × 10^{-14} erg cm^{-2} s^{-1}), respectively. The APM finding charts show a faint object (R_{mag} = 21.74, $B-R < 1.74$) located close to the X-ray source position (Δ = 4″ from the HRI position). If the HRI and PSPC detected sources are due to the same object and the spectral model is right, RX J122802.3+440803 is time variable and a background AGN could explain the optical and X-ray appearance.

The other source (RX J122747.8+440209, H2) was only visible during the HRI observation (cf. Fig. 1) at α = 12^{h}27^{m}47^s.8, δ = 44°02′09″ with a count rate of $(4.8 \pm 0.2) \times 10^{-4}$ cts s^{-1} (f_x = 1.8 × 10^{-14} erg cm^{-2} s^{-1}). For the PSPC observation we calculate an upper limit (2σ) of 1.3×10^{-3} cts s^{-1} (f_x = 1.7 × 10^{-14} erg cm^{-2} s^{-1}, background from a ring with 30″ to 50″ diameter). This upper limit is comparable to the detected HRI flux. No counterpart was suggested by the APM finding charts.

4.4. Separating point source and diffuse emission components

4.4.1. HRI measurement

We collected all counts within the D_{25} ellipse of NGC 4449 to calculate the integrated luminosity of NGC 4449. The background was determined in a ring from 7′ to 10′ diameter around the center of the galaxy (point sources in this region were removed). 580 ± 38 counts associated with NGC 4449 remained. The detected point sources listed in Table 2 account for 277 ± 18 counts (count rate (18.2 ± 1.2) cts s^{-1}), thus we detect 303 ± 42 counts (count rate (19.7 ± 2.7) cts s^{-1}) due to unresolved emission. The latter may be composed of X-ray emission from unresolved point-like sources and from a hot gaseous component. The luminosity of the resolved point sources is $L_x(point)$ = $(1.1 \pm 0.1) \times 10^{39}$ erg s^{-1} for a 5 keV thermal bremsstrahlung model. Spectral investigations of the integral point source spectra with the PSPC favor either a 0.9 keV thermal bremsstrahlung (BR) or a power law (PO) model with index 2.5 (cf. Sect. 4.4.2). The conversion factor for the 0.9 keV BR model is nearly identical to the 5 keV BR model, for the PO model we obtain a luminosity of $L_x(point)$ = $(1.4 \pm 0.2) \times 10^{39}$ erg s^{-1}. The luminosity of the extended component is estimated at $L_x(ext)$ = $(1.1 \pm 0.2) \times 10^{39}$ erg s^{-1} for a thin thermal plasma spectrum with T = 0.3 keV. From our HRI measurement we then end up with a total X-ray luminosity (0.1-2.4 keV) for NGC 4449 of $L_x(total)$ = $(2.1 - 2.5) \times 10^{39}$ erg s^{-1}.

4.4.2. PSPC measurement

The PSPC soft and hard1 maps show extended emission components (cf. Fig. 3). To study, if this emission is due to unresolved point sources or due to 'real' diffuse emission (e.g. a hot plasma), we used the spectral capabilities of the ROSAT PSPC. Two different spectra were extracted. In a first spectrum we have collected all photons around point sources with a cut diameter of 60″ (HRI positions used), the corresponding extraction area is called *region 1*. All remaining photons inside the D_{25} ellipse of the galaxy were assigned to a second spectrum (*region 2*). The background (calculated in an area as explained in Sect. 4.4.1) subtracted spectra were binned with a signal to noise ratio $S/N \geq 5$ and contained in total 655 ± 27 and 320 ± 24 photons for *region 1* and *2*, respectively.

We fitted simple power law (PO), thermal bremsstrahlung (BR), and thin thermal plasma (TH) models to the spectra. Table 5 gives the results for both regions. We give 1σ errors. Spectral investigations of *region 1* favor absorbed PO or BR models, while a TH spectrum may be rejected due to the high χ^2/ν. A power law index of 2.5 or a temperature of ∼1 keV in the PO and BR model indicate the hard spectral behavior of the X-ray sources in *region 1*. Both models predict integral point source luminosities of $L_x \approx 1.6 \times 10^{39}$ erg s^{-1} (corrected for Galactic absorption). The measured absorption for the PO and BR model exceed the Galactic foreground by 4.0×10^{20} cm^{-2}

Table 5. Spectral investigation of point sources (region 1) and extended emission components (region 2) in NGC 4449

			N_H (10^{20} cm^{-2})	Index	T (keV)	ν	χ^2/ν	$f_x^{\S}$ (10^{-13} erg cm^{-2} s^{-1})	$L_x^{\S}$ (10^{39} erg s^{-1})
ONE COMPONENT MODELS*									
region 1 ♣									
		PO	$5.2^{+1.0}_{-0.9}$	$2.50^{+0.24}_{-0.27}$		19	1.5	10.6 ± 0.7	1.7
		BR	$3.5^{+0.6}_{-0.6}$		$0.89^{+0.26}_{-0.16}$	19	1.4	10.0 ± 0.2	1.6
		TH	$1.2^{\sharp}$		1.1 ± 0.1	19	5.8	6.4 ± 1.4	1.0
region 2 ♠									
		PO	$6.6^{+1.9}_{-1.7}$	$3.8^{+0.5}_{-0.6}$		7	1.8	5.6 ± 0.5	0.9
		BR	$3.5^{+1.2}_{-1.2}$		$0.37^{+0.14}_{-0.07}$	7	1.6	5.0 ± 0.4	0.8
		TH	$1.2^{\sharp}$		0.25 ± 0.03	7	2.5	5.1 ± 0.5	0.8
TWO COMPONENT MODELS *									
region 1 ♣									
	model 1	PO	5.2^{fix}	2.5^{fix}		19	1.2	9.2 ± 2.2	1.5
		+TH	5.2^{fix}		0.55 ± 0.55			1.1 ± 1.1	0.2
	model 2	PO	5.2^{fix}	2.5^{fix}		19	1.1	8.5 ± 2.4	1.4
		+TH	1.2^{fix}		0.50 ± 0.36			1.6 ± 1.5	0.3
region 2 ♠									
	model 1	PO	5.2^{fix}	2.5^{fix}		7	1.9	2.6 ± 0.8	0.4
		+TH	5.2^{fix}		0.14 ± 0.03			3.1 ± 1.2	0.5
	model 2	PO	5.2^{fix}	2.5^{fix}		7	1.0	1.2 ± 0.4	0.2
		+TH	1.2^{fix}		0.25 ± 0.04			4.2 ± 2.1	0.7

* PO: power law, BR: thermal bremsstrahlung, TH: thin thermal plasma

§ 0.1–2.4 keV band, corrected for Galactic absorption

♣ extracting all photons with a cut diameter of 60′′ around the position of detected point sources (positions according to Table 2) and merging them to a spectrum (22 spectral bins)

♠ remaining photons within the D_{25} ellipse of NGC 4449 (10 spectral bins)

♯ lower boundary fixed to Galactic foreground

fix value fixed

and 2.3×10^{20} cm^{-2}, respectively. These values are comparable with radio measurements of the HI disk and halo of NGC 4449 (Bajaja et al. 1994). Inside the D_{25} ellipse of NGC 4449 the HI column measured with an aperture of a few arcmin varies from $N_H \sim 4 \times 10^{20}$ cm^{-2} to $N_H \sim 5 \times 10^{20}$ cm^{-2}. One component models fitted to *region 2* predict softer spectral behavior (PO index of 3.8; temperatures of $T = 0.37$ keV for the BR, and $T = 0.25$ keV for the TH model). Independent of the model the X-ray luminosities are around 8×10^{38} erg s^{-1}.

To first order, the spectrum of *region 1* seems to be dominated by the hard spectra of point sources, the one of *region 2* by soft emission components. The soft emission components may consist of the superposition of unresolved point sources and a possible hot gaseous component of the interstellar medium. In addition the more extended PSF of the PSPC soft band compared to the hard band may smear out soft emission components of the detected point sources into *region 2*.

Neither for *region 1* nor for *region 2* the deduced χ^2/ν values are near to 1.0, indicating more complex spectra in both regions. In a two component model we assumed that both spectra are the superposition of a PO spectrum caused by point sources and a TH spectrum caused by a hot gaseous component of the interstellar medium or unresolved sources with thermal spectra, which are related to the hot interstellar medium (e.g. superbubbles and SNRs). Since the number of source counts restricted us to a low number of free parameters we fixed the absorption and the spectral slope of the PO part to the results of the one component PO model fitted to *region 1* which seemed to be dominated by point sources. The absorption of the TH part was either fixed to the value of the PO part (*model 1*: the thermal part is originating in the disk of the galaxy) or to the

Galactic foreground (*model 2*: the thermal part is associated with the outer disk or a thermal component in the halo of the galaxy). For both regions the resulting χ^2/ν values were better for *model 2* (1.1 and 1.0). The luminosity of point sources in *region 1* is estimated at 1.4×10^{39} erg s^{-1}, contributions of the thermal part at 3×10^{38} erg s^{-1} (corresponding to a surface brightness of $S_x = 6 \times 10^{37}$ erg arcmin^{-2} s^{-1}). The ratio of the emission measure of the components strengthens our assumption that *region 1* is dominated by point source contributions. In opposite, in *region 2* (unresolved) point sources contribute 2×10^{38} erg s^{-1} while the TH part contributes 7×10^{38} erg s^{-1} ($S_x = 6 \times 10^{37}$ erg arcmin^{-2} s^{-1}). The better χ^2/ν values for *model 2* compared to *model 1* may argue that we measure X-ray emission from a thermal component originating above the HI disk of NGC 4449; that gives an indication for a possible detection of gas ejected from the disk into the halo of the galaxy. Spectral analysis of *region 2* suggests a temperature of the gas around 0.25 keV (2.9×10^6 K), while the temperature is a factor of two higher in *region 1*. The latter estimate contains a greater error, since the flux of this component is lower. Accepting the difference as real and not due to systematic errors, we probably detect hotter gas related to outflow from active regions (e.g. superbubbles) into the outer disk of the galaxy. However one always has to keep in mind that our assumptions for the absorption and of a one temperature model for the hot interstellar medium are certainly oversimplified.

The results obtained by spectral analysis of the NGC 4449 PSPC data may be compared to the results of Sect. 4.1. The spectral result for point sources in *region 1* ($L_x = 1.4 \times 10^{39}$ erg s^{-1}) should be equivalent to the results of the 'multi source fit technique' (cf Sect. 4.1 and Table 3). Integrating the count rates and using a energy conversion factor for the assumed PO model (1.12×10^{-11} erg cm^{-2} cts^{-1} corrected for Galactic absorption), one obtains 1.1×10^{39} erg s^{-1}. The remaining difference may be due to unresolved point sources in the extracted region or errors introduced by the integral spectral model.

The PSPC measured luminosity for resolved point source contributions (PO part of *region 1* gives $L_x = 1.4 \times 10^{39}$ erg s^{-1}) is in agreement with the HRI result of this component calculated in Sect. 4.4.1. Unresolved emission in the PSPC image (TH part of *region 1* and whole luminosity of *region 2* yield $L_x = 1.2 \times 10^{39}$ erg s^{-1}) also agrees with unresolved emission components measured with the HRI (cf. Sect. 4.4.1).

5. Discussion

5.1. The supernova remnant (X4)

A couple of SNe with X-ray luminosities exceeding 10^{38} erg s^{-1} have been reported for spiral galaxies; e.g. in NGC 891 (SN 1986J, $L_x = 6 \times 10^{39}$ erg s^{-1}, Bregman & Pildis 1994), in NGC 6946 (SN 1980K, $L_x = 2.8 \times 10^{39}$ erg s^{-1}, Schlegel 1994a,b), or NGC 1313 (SN 1978K, $L_x \sim 10^{40}$ erg s^{-1}, Colbert et al. 1995). Schlegel (1995) reviews several theoretical explanations for the high luminosities (pulsar input, a reverse shock running back into the expanding debris of the SN, or a outgoing shock crushing of cloudlets in the debris field). Blair et al. (1983) used optical measurements to estimate the absorbing column towards the SNR in NGC 4449 to $N_H = 1.5 \times 10^{21}$ cm^{-2} which is in good agreement with our lower limit. With help of other SNRs, for which the temperatures are known, Blair et al. estimated the temperature of X4 at 6×10^6 K, which again is close to our spectral results. For further analysis we assume $T = 7 \times 10^6$ K and $N_H = 1.5 \times 10^{21}$ cm^{-2}. The ROSAT HRI measurement leads to an intrinsic luminosity of $L_x = (4.7 \pm 0.6) \times 10^{38}$ erg s^{-1} which agrees within the errors with the *Einstein* HRI luminosity of $L_x = 4.4 \times 10^{38}$ erg s^{-1} measured by Blair et al. (corrected for the different energy bands) giving further support to the SNR identification, an X-ray source class for which no time variability one short time scales (tens of years) is expected.

Blair et al. estimated the age of the the SNR in NGC 4449 to ~ 100 yr and explained the high X-ray luminosity by explosion of a massive star into a high density (25 cm^{-3}) medium. Such a density can be reached in the shells of superbubbles (McCray & Kafatos 1987). Possible heating mechanisms proposed are ISM dominated reverse shocks, ejecta dominated reverse shocks, or blast waves.

5.2. Diffuse emission

The averaged surface brightness for the TH component measured with the PSPC, possibly representing the hot interstellar medium in the outer disk/halo of NGC 4449 is $S_x = 6 \times 10^{37}$ erg arcmin^{-2} s^{-1}. This is in good agreement with measurements of edge-on galaxies showing diffuse X-ray emission out of the halo, like NGC 4631 (Vogler & Pietsch 1996), NGC 253 (Pietsch & Trümper 1993), NGC 4565 (Vogler et al. 1996a), NGC 3628 (Dahlem et al. 1996), or Arp 220 (Heckman et al. 1996). The interacting galaxy NGC 4631 is known for widespread star formation in its disk. It shows a surface brightness of $S_x = 4.5 \times 10^{37}$ erg arcmin^{-2} s^{-1} in the northern halo hemisphere; and $S_x = 1.5 \times 10^{37}$ erg arcmin^{-2} s^{-1} in the southern halo hemisphere. The southern hemisphere may be shadowed (at least partly) by the HI disk of the galaxy. Wang et al. (1995) established a temperature of the halo gas of 3×10^6 K from ROSAT PSPC observations and found in addition indications for a cooler component. The temperature of their one component model is in agreement with our temperature of 2.5×10^6 K for NGC 4449 and may also be compared to NGC 253. The central starburst in NGC 253 is traced with the ROSAT HRI and the PSPC hard bands. Emission out of the halo of NGC 253 is detected in the 0.1–0.4 keV soft band with a temperature of $\lesssim 2 \times 10^6$ K. NGC 4565 is not known to be an active or starburst galaxy. The measured diffuse halo brightness ($S_x = 3.9 \times 10^{37}$ erg arcmin^{-2} s^{-1}) may be interpreted as sign of past activity if one takes into account the long cooling time of the X-ray gas.

For NGC 4449 the hard1 band of the ROSAT PSPC showed a circular region of diffuse emission centered $\sim 1'$ north of the center of the galaxy and protruding to the northern periphery of the galaxy (cf. Fig. 3). The diffuse emission may arise from hot

gas thrown out from the actual starburst. The PSPC soft band, tracing a cooler gaseous component, shows contributions from the northern part and, in a less degree, from the southern part of the galaxy. Possibly a part of the soft band emission (especially the southern part) is due to gas thrown out in an 'older' starburst phase and cooled down in the meantime.

Attributing the whole TH components ($L_x = 1.0 \times 10^{39}$ erg s^{-1}) in the spectra of Sect. 4.4.2 to hot gas in the outer disk and halo one may estimate the density, mass, and cooling time of the X-ray gas (assuming an average temperature of $\sim 3 \times 10^6$ K for the gas contained in a hemisphere above the disk). For thermal cooling, a spherical gas cloud of homogeneous density and radiation equilibrium (Nulsen et al. 1984), we derive $n_e \simeq 4 \times 10^{-3}$ cm$^{-3}/\sqrt{\eta}$, $m \simeq 6 \times 10^8$ M$_\odot \times \sqrt{\eta}$, and $\tau_c \simeq 2 \times 10^8$ yr $\times \sqrt{\eta}$ assuming a free filling factor η (this filling factor may be understood as representing the fraction of the disk volume harboring chimney activities).

Hill et al. (1994) give three time scales of starburst phases for NGC 4449: 2×10^6 yr, 4×10^7 yr, and 2×10^9 yr. For reasonable filling factors ($\eta \gtrsim 5\%$), the cooling time τ_c of the X-ray gas would be long enough that the gas could have been heated and ejected from the disk within the two preceding star forming episodes.

5.3. Comparison to the Magellanic Clouds

Our results obtained for the Magellanic-type irregular galaxy NGC 4449 may be compared to X-ray observation of the Large Magellanic Cloud (LMC) which also shows ongoing star formation and the Small Magellanic Cloud (SMC). A detailed reanalysis of the *Einstein* observations of the LMC and SMC is given in Wang et al. (1991) and Wang & Wu (1992), respectively. A total of 105 (75) point sources are located inside the optical extent of the LMC (SMC). 57 (25) of these have been identified with sources in the LMC (SMC). For both galaxies about one half of the sources are SNRs, $\sim$ 20% are X-ray binaries, and the remaining sources are associated with OB associations and H II regions in the Clouds. Neither for the LMC nor the SMC a point like source was associated with the position of the center of the galaxy. This is in agreement with the expectations, since Magellanic-type galaxies do not possess a clear defined nucleus as normal spiral galaxies do. The authors point out that there is a close correlation of X-rays from SNRs and high mass X-ray binaries with Hα regions in the Magellanic Clouds, which trace out recent star formation in the galaxy. This seems also to be true for NGC 4449 (cf. Fig. 5 and Sect. 4.3) and may reflect that the X-ray emission in the Magellanic-type galaxies is dominated by Population I components. Young Population I objects make up the population of OB associations, which are expected to form cavities in the ISM via stellar winds and multiple SN explosions (McCray & Kafatos 1987) that are filled with hot gas. Therefore one expects a correlation of these objects with the detection of hot interstellar medium (Norman & Ikeuchi 1989). We showed that the X-ray spectrum of NGC 4449 may be interpreted as a superposition of resolved and unresolved point sources and diffuse emission from hot coronal gas (cf. Sect. 4.4 and 5.2). For the diffuse component we estimated a mean temperature of $T \sim 3 \times 10^6$ K.

For the LMC Wang et al. (1991) report a hot diffuse component. Similar to NGC 4449 the LMC orientation is face-on, and the measured temperature of the hot ISM was between 3×10^6 K and 10^7 K, the highest temperature was associated with the 30 Doradus region. Diffuse X-ray emission from the 30 Doradus region was already detected in the ROSAT PSPC 'first light' pointings (Trümper et al. 1991). ROSAT all sky survey images (Pietsch & Kahabka 1993) and images of ROSAT PSPC pointed observations put together as a mosaic (Snowden & Petre 1994) clearly reveal diffuse emission with a wealth of detailed structure on angular scales from arc minutes to a few degrees (15 pc to a few kpc in the LMC). The fraction of point source components to diffuse components is comparable for NGC 4449 and the LMC: In the case of NGC 4449 the total point source luminosity is estimated to 1.7×10^{39} erg s^{-1}, the luminosity of the diffuse component to 9×10^{38} erg s^{-1}. For the LMC the point source component is $\sim 3 \times 10^{38}$ erg s^{-1} and the diffuse component $\sim 2 \times 10^{38}$ erg s^{-1}. The luminosity of the components seems to scale with the masses of the LMC and NGC 4449 (2 and 7 $\times 10^9$ M$_\odot$, respectively (Schommer et al. 1992; Bajaja 1994)).

In their investigation of X-ray emission from giant H II regions in the spiral galaxy M101 (distance 6 Mpc) Williams & Chu (1994) tried to shed light onto the nature of the objects involved by comparing them with the better understood objects. Their first choice was the prototypical H II region 30 Doradus in the LMC. We will follow their argumentation to get a better understanding for our star forming regions in NGC 4449. From ROSAT PSPC pointings of the 30 Dor region (cf. Williams & Chu and references therein) an X-ray luminosity of 10^{37} erg s^{-1} was detected for the inner 600 pc diameter region, the point sources in this region are one superbubble, two SNRs, and two X-ray binaries. Shifting the region from the distance of the LMC (d = 50 kpc) to the distance of NGC 4449 (d = 3.7 Mpc) the viewing angle would be comparable to the FWHM of the ROSAT PSPC. The ROSAT HRI would provide the necessary angular resolution to resolve the region, however the point source detection limit in the case of NGC 4449 ($\sim 5 \times 10^{37}$ erg s^{-1}) is above the luminosity of the whole inner region. An X-ray binary similar to LMC X-1 ($L_x = 1.5 \times 10^{37}$ erg s^{-1}), which is located near the inner region of 30 Dor, would still be visible as a point like source at the distance of NGC 4449. From this one might expect for the observation of star forming regions in NGC 4449 the detection of bright point like sources, surrounded by extended emission caused by individual faint point sources. For some of these point sources, the SNRs and superbubbles, thermal spectra with temperatures in the range of several 10^6 K are expected. We already pointed out that such sources might cause a considerable fraction of the thermal component measured in the two component spectra of Sect. 4.4.2.

6. Summary

The results of the ROSAT HRI and PSPC observations of NGC 4449 may be summarized a follows:

◇ The total X-ray emission measured inside the D_{25} ellipse of NGC 4449 is $L_x \sim 2.5 \times 10^{39}$ erg s^{-1} for both detectors (0.1–2.4 keV ROSAT band, corrected for Galactic absorption).

◇ Seven point like sources inside the D_{25} ellipse are resolved by the ROSAT HRI and contribute an integral luminosity of $L_x \sim 10^{39}$ erg s^{-1}, the individual luminosities range from 7×10^{37} erg s^{-1} to 3×10^{38} erg s^{-1}). The center of the galaxy is detected as a point-like source ($L_x \sim 10^{38}$ erg s^{-1}). A bright source is located at the position of a young SNR (intrinsic $L_x = 4.7 \times 10^{38}$ erg s^{-1}). Another bright source ($L_x \sim 3 \times 10^{38}$ erg s^{-1}) is positioned between the boundaries of a double Hα shell.

◇ Extended emission features are visible in an adaptive filtered HRI map as well as in the PSPC 0.1–0.4 keV and 0.5–0.9 keV maps. The emission may consist of two ingredients: unresolved point sources and diffuse emission from hot interstellar medium. We tried to distinguish (resolved and unresolved) point source components from diffuse emission components with the help of the spectral capabilities of the ROSAT PSPC. Two component spectra (power law and thin thermal plasma) suggest a luminosity of 1.6×10^{39} erg s^{-1} for (resolved and unresolved) point sources in the galaxy (power law), while the remaining X-ray emission ($L_x = 1.0 \times 10^{39}$ erg s^{-1}) is described by the thin thermal plasma component. The thermal component may originate from hot interstellar medium in the outer disk and/or halo of the galaxy created during the star forming episodes 2×10^6 years and 4×10^7 years ago. However, the limited spectral resolution of the ROSAT PSPC as well as the face-on orientation of the galaxy do not allow to separate the components spatially.

◇ The X-ray emission components of NGC 4449 may be understood by projecting the emission regions of the starforming Magellanic galaxy LMC to the distance of NGC 4449 (scaled for the different galaxy masses).

Acknowledgements. We thank our colleagues from the MPE ROSAT group for their support. This research has made use of the SIMBAD database operated at CDS, Strasbourg and of data obtained through the High Energy Astrophysics Science Archive Research Center Online Service, provided by the NASA-Goddard Space Flight Center. The ROSAT project is supported by the German Bundesministerium für Bildung, Wissenschaft, Forschung und Technologie (BMBF/DARA) and the Max-Planck-Gesellschaft (MPG).

References

Bajaja E., Huchtmeier W.K., Klein U., 1994, A&A 285, 385
Balick B., Heckman T., 1978, ApJ 226, L7
Blair W.P., Kirshner R.P., Winkler P.F., 1983, ApJ 272, 84
Blair W.P., Raymond J.C., Fesen R.A., Gull T.R., 1984, ApJ 279, 708
Bothun G.D., 1986, AJ 91, 507
Bregman J.N., Pildis R.A., 1994, ApJ 420, 570
Colbert E.J.M., Petre R., Schlegel E.M., Ryder S.D., 1995, ApJ 446, 177
Condon J.J., 1987, ApJS 65, 485
Cruddace R.G., Hasinger G.R., Schmitt J.H.M.M., 1988, in: Murtagh F., Heck A. (eds.) Astronomy from large databases, ESO Conference and Workshop Proc. 28, p. 177
Dahlem M., Heckman T.M., Fabbiano G., Lehnert M.D., Gilmore D., 1996, ApJ 461, 724
Dickey J.M., Lockman F.J., 1990, ARA&A 28, 215
Fabbiano G., Kim D.-W., Trinchieri G., 1992, ApJS 80, 531
Heckman T.M., Dahlem M., Eales S.A., Fabbiano G., Weaver K., 1996, ApJ 457, 616
Hill R.S., Home A.T., Smith A.M., Bruhweiler F.C., Cheng K.P., Hintzen P.M.N., Oliversen R.J., 1994, ApJ 430, 568
Hunter D.A., 1984, ApJ 276, L35
Hunter D.A., Gallagher J.S., 1990, ApJ 362, 480
Hunter D.A., Gallagher J.S, 1992, ApJ, 391, L9
Irwin M., Maddox S., McMahon R., 1994, Spectrum 2, 14
McCray R., Kafatos M., 1987, ApJ 317, 190
Norman C.A., Ikeuchi S., 1989, ApJ 345, 372
Nulsen P.E.J., Stewart G.C., Fabian A.C., 1984, MNRAS 208, 185
Pietsch W., Trümper J., 1993, Adv. Sp. Res. 13, (12) 171
Pietsch W., Kahabka P., 1993, in: Baschek B., Klare G., Lequeux J. (eds.) New aspects of Magellanic Cloud research, Lect. Notes in Phys. 416, p. 71
Sabbadin F., Ortolani S., Bianchini A., 1984, A&A 131, 1
Schlegel E.M., 1994a, ApJ 424, L99
Schlegel E.M., 1994b, ApJ 434, 523
Schlegel E.M., 1995, Rep. Prog. Phys. 58, 1375
Seaquist E.R., Bignell R.C., 1978, ApJ 226, L5
Schommer R.A., Suntzeff N.B., Olszewski E.W., Harris H.C., 1992, AJ 103, 447
Snowden S.L., Petre R., 1994, ApJ 436, L123
Trümper J., 1983, Adv.Space Res. 2, 241
Trümper J., Hasinger G., Aschenbach B., et al., 1991, Nat 349, 579
Tully R.B., 1988, Nearby Galaxies Catalog, Cambridge University Press, Cambridge
Voges W., Gruber R., Paul J., et al., 1992, in: Guyenne T.D., Hunt J.J. (eds.) Proc. European ISY conference, ESA ISY-3, p. 223
Vogler A., Pietsch W., 1996, A&A 311, 35
Vogler A., Pietsch W., Kahabka P., 1996a, A&A 305, 74
Vogler A., Pietsch W., Bertoldi F., 1996b, A&A, in press
Wang Q., Hamilton H., Helfand D.J., Wu X., 1991, ApJ 374, 475
Wang Q., Wu X., 1992, ApJS 78, 391
Wang Q.D., Walterbos R.A.M., Steakley F.M., Norman C.A., Braun R., 1995, ApJ 439, 176
Williams M.R., Chu Y.-H., 1995, ApJ 439, 132
Zimmermann H.-U., Belloni T., Boese G., et al., 1992, in: Guyenne T.D., Hunt J.J. (eds.) Proc. European ISY conference, ESA ISY-3, p. 231
Zimmermann H.-U. et al., 1994, "EXSAS User Guide", 4th edition

This article was processed by the author using Springer-Verlag LaTeX A&A style file *L-AA* version 3.